



Lambda polarization at the Electron-ion collider in China

Zhaohuizi Ji¹ · Xiao-Yan Zhao¹ · Ai-Qiang Guo² · Qing-Hua Xu¹ · Jin-Long Zhang^{1,3}

Received: 12 August 2023 / Revised: 30 August 2023 / Accepted: 30 August 2023 / Published online: 27 October 2023

© The Author(s), under exclusive licence to China Science Publishing & Media Ltd. (Science Press), Shanghai Institute of Applied Physics, the Chinese Academy of Sciences, Chinese Nuclear Society 2023

Abstract

Lambda polarization can be measured through its self-analyzing weak decay, making it an ideal candidate for studying spin effects in high-energy scattering. In lepton-nucleon deep inelastic scattering (DIS), Lambda polarization measurements can probe polarized parton distribution functions (PDFs) and polarized fragmentation functions (FFs). One of the most promising facilities for high-energy nuclear physics research is the proposed Electron-ion collider in China (EicC). As a next-generation facility, EicC is set to advance our understanding of nuclear physics to new heights. In this article, we study the Lambda production in electron-proton collisions at the EicC energy, in particular the reconstruction of Lambda based on the performance of the designed EicC detector. In addition, taking spontaneous transverse polarization as an example, we provide a theoretical prediction with a statistical projection based on one month of EicC data, offering valuable insights into future research prospects.

Keywords Electron-ion collider in China · Lambda polarization · Polarizing fragmentation functions · Nucleon structure

1 Introduction

Spin is a fundamental particle property that plays a critical role in the advancement of modern physics. A growing number of experimental findings, such as the spontaneous transverse polarization of Λ and the proton spin crisis, have demonstrated that there is significantly more to be understood about spin behavior in high-energy reactions. The Lambda hyperon ($\Lambda/\bar{\Lambda}$) has emerged as an exceptionally powerful tool in spin physics, primarily owing to its parity-violating weak decay, which results in a nonuniform angular distribution of its products with respect to the $\Lambda(\bar{\Lambda})$

spin direction [1]. In high-energy reactions, $\Lambda(\bar{\Lambda})$ is abundantly produced and efficiently detected via the decay channel $\Lambda \rightarrow p\pi^-$ ($\bar{\Lambda} \rightarrow \bar{p}\pi^+$) (branching ratio is 63.9%). In the $\Lambda(\bar{\Lambda})$ rest frame, the decay protons are preferentially emitted along the polarization direction of their parent Λ with the following angular distribution:

$$\frac{dN}{d\cos\theta^*} \propto \mathcal{A} \left(1 + \alpha_{\Lambda(\bar{\Lambda})} P_{\Lambda(\bar{\Lambda})} \cos\theta^* \right), \quad (1)$$

where \mathcal{A} is the detector acceptance, $\alpha_{\Lambda} = 0.732 \pm 0.014$ is the weak decay parameter [2], θ^* is the angle between the proton momentum direction and the $\Lambda(\bar{\Lambda})$ polarization direction in the Λ rest frame.

The spontaneous transverse polarization of Λ was first observed in 1976 in the unpolarized proton beam scattering on a beryllium target [3], where perturbative Quantum Chromodynamics (QCD) only predicted a negligible polarization [4]. These puzzling results triggered a series of theoretical and phenomenological studies that extended far beyond Λ polarization. Experimentally, measurements of $\Lambda(\bar{\Lambda})$ polarization have since been extensively explored in various high-energy processes, including electron-positron annihilation [5–7], lepton-nucleon deeply inelastic scattering (DIS) [8–10], hadron-hadron scattering [11–13], and heavy ion collisions [14–18], yielding invaluable insights into numerous aspects of physics. These measurements have

This work was supported by the National Natural Science Foundation of China (Nos.12275159, 12075140, and 12175117), 100 Talents Program of CAS, and Shandong Provincial Natural Science Foundation (No. ZFJH202303).

✉ Jin-Long Zhang
jlzhang@sdu.edu.cn

¹ Institute of Frontier and Interdisciplinary Science, Shandong University, Qingdao 266237, China

² Institute of Modern Physics of CAS, Lanzhou 730000, China

³ Southern Center for Nuclear-Science Theory (SCNT), Institute of Modern Physics, Chinese Academy of Sciences, Huizhou 516000, China

served diverse purposes, including unraveling the physical origins of spontaneous polarization, understanding the nucleon spin structure, comprehending spin effects in the fragmentation processes, and exploring extreme conditions of high density and high temperature in heavy-ion collisions.

High-precision $\Lambda(\bar{\Lambda})$ polarization measurements in the proposed electron-ion collider provide unique opportunities to study spin-dependent fragmentation functions (FFs) and polarized parton distribution functions (PDFs) [19–26]. The Electron-ion collider in China, EicC, is the proposed next-generation high-energy nuclear physics facility based on the High Intensity heavy-ion Accelerator Facility (HIAF) in Huizhou, China [27, 28]. It is conceptually designed to deliver high luminosity electron-proton, electron-ion collisions with highly polarized electron, proton, and light-ion beams. With a complementary kinematics coverage to other electron-ion collider proposals worldwide [29–31], the featured physics at the EicC includes a 3-dimensional proton spin structure, nuclear partonic structure, and exotic hadron states, *etc.* $\Lambda(\bar{\Lambda})$ polarization measurements at the EicC are expected to be sensitive not only to spin-dependent parton distribution functions but also to spin-dependent fragmentation functions. Potential measurements of the $\Lambda(\bar{\Lambda})$ transverse polarization and impact studies have been performed for the US-based EIC, which are designed to collide with electron and proton/ion beams at significantly higher energies than EicC [26].

In this article, the $\Lambda(\bar{\Lambda})$ production in electron-proton scattering under the EicC configuration was studied. Based on the current conceptual EicC detector design, especially that of the tracking subsystem, the reconstruction performance for $\Lambda/\bar{\Lambda}$ is assessed. In Sect. 2, the simulation setup including the event generator used is described, as well as the detector configuration and corresponding fast simulation procedure. The performance of the $\Lambda/\bar{\Lambda}$ reconstruction is presented in Sect. 3. In Sect. 4, considering the spontaneous transverse polarization as an example, the potential statistical precision for the polarization measurements is presented along with the theoretical predictions. A brief summary and outlook are provided in Sect. 5.

2 Simulation framework

To simulate the $\Lambda(\bar{\Lambda})$ production in electron-proton scattering, the event generator PYTHIAeRHIC [32], a modified version of PYTHIA6.4.28 [33], was used with the parton distribution functions (PDFs) input from LHAPDF [34]. The collision energy chosen was the baseline energy outlined in the EicC whitepaper [28], which was a 3.5 GeV electron on a 20 GeV proton. The leading-order diagram for the

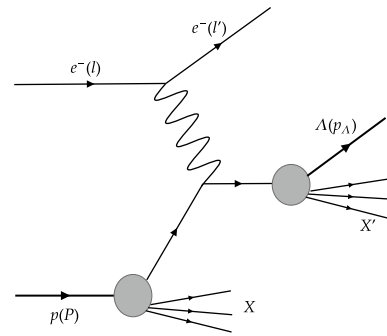


Fig. 1 Leading-order diagram for Λ production in a semi-inclusive DIS process

Λ production in the DIS process is shown in Fig. 1. The kinematics of the studied DIS events were constrained to the following ranges: Bjorken- x $10^{-3} < x_B < 1$, transferred 4-momentum squared $Q^2 > 1 \text{ GeV}^2$, and hadronic invariant mass squared $W^2 > 4 \text{ GeV}^2$. Ten million DIS events were generated in the subsequent studies.

At the generator level, the average number of Λ produced per DIS event in the kinematic range indicated above was approximately 0.1. In the laboratory frame, the momentum and polar angle distributions for Λ and the decay products are shown in Fig. 2. Comparing the distributions of the daughter proton and pion with Λ , protons are found to carry most of the Λ momentum whereas pions only share a small fraction. Λ is preferentially produced in the proton-going direction, with a large amount produced at a significantly forward angle. The same distributions shown in Fig. 2 for $\bar{\Lambda}$ are similar with slight differences, which are discussed later.

In this study, we are mostly interested in the $\Lambda/\bar{\Lambda}$ from the struck quark fragmentation (current fragmentation region). Typically, Feynman- x is an effective variable for separating the current target fragmentation regions. Feynman- x x_F is defined as $x_F \equiv 2p_L^{\Lambda(\bar{\Lambda})}/W$, where $p_L^{\Lambda(\bar{\Lambda})}$ is the $\Lambda(\bar{\Lambda})$ longitudinal momentum in the hadronic center of the mass frame, and W is the hadronic invariant mass. The criteria $x_F > 0$ is expected to suppress the contributions from the target fragmentation region. The correlations between Feynman- x and $\Lambda/\bar{\Lambda}$ pseudorapidity η are shown in the upper panels of Fig. 3. Here, pseudorapidity is defined as $\eta = -\ln(\tan(\theta/2))$, where θ is the polar angle. Following the EicC convention, a positive η is along the moving direction of the proton/ion beam. It can be observed that $\Lambda/\bar{\Lambda}$ with $x_F < 0$ is mostly produced in the significantly forward region, which is discarded in the following simulation and analysis. Considering the limited coverage of the EicC central detector, $|\eta| < 3$ was applied to $\Lambda/\bar{\Lambda}$ and their daughter particles. The transverse momentum p_T versus η for Λ and $\bar{\Lambda}$ with $x_F > 0$ and

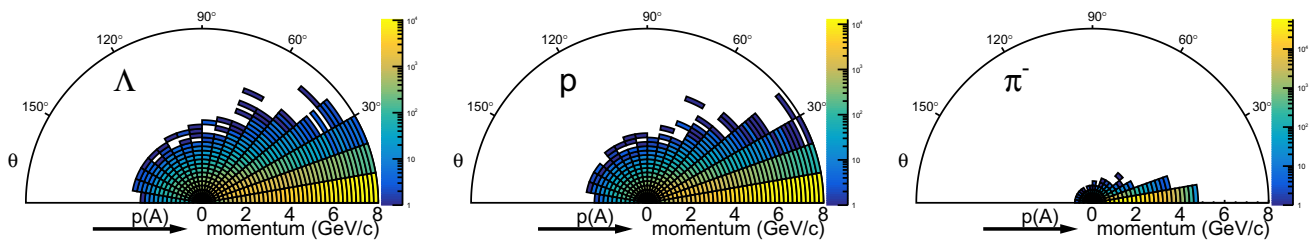
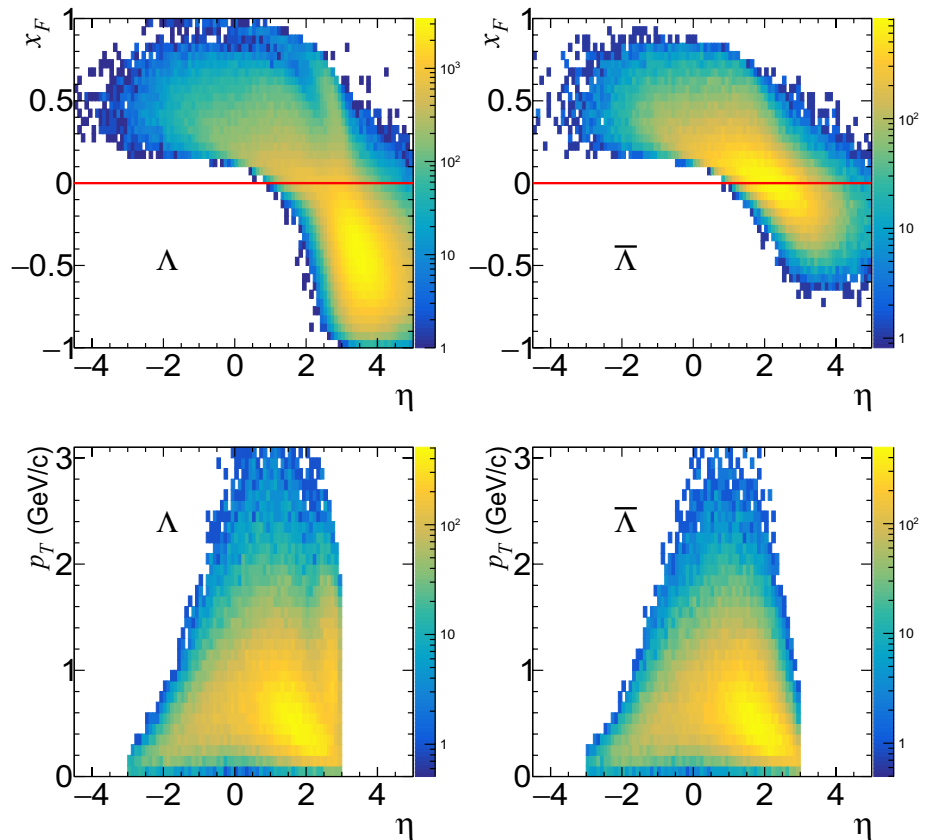


Fig. 2 (Color online) Momentum (radial) and polar angle (polar) distributions for Λ and its decay products in the laboratory frame

Fig. 3 (Color online) Upper panels: Feynman- x x_F versus The pseudorapidity η for Λ (left) and $\bar{\Lambda}$ (right) in the laboratory frame. Only $\Lambda/\bar{\Lambda}$ above the red line ($x_F > 0$) are retained. Lower panels: transverse momentum p_T versus the pseudorapidity η for Λ (left) and $\bar{\Lambda}$ (right) with $x_F > 0$ and $|\eta| < 3$ (also $|\eta| < 3$ for the daughter proton and pion)



$|\eta| < 3$, are shown in the lower panels of Fig. 3. By tracing the full record of events in PYTHIA, the origins of $\Lambda/\bar{\Lambda}$ are shown in Fig. 4. At the EicC energy, approximately half of $\Lambda/\bar{\Lambda}$ originates from the decay of heavier hyperons. There are also significant contributions from the beam remnants (di-quarks). In this study, we do not separate the different sources of $\Lambda/\bar{\Lambda}$.

The preliminary conceptual design of the EicC detector has been described in white papers [27, 28]. From the inner to outer parts, it consists of a vertex/tracking detector, particle identification (PID) system, and calorimeter system, etc. For the Λ measurement, the most relevant parts were the tracking and PID systems. The latest EicC tracking detector design is described in Ref. [35]. Current tracking

system designs use hybrid models. For the middle rapidity ($|\eta| < 1.1$), there are 5 layers of silicon and 4 layers of micro-pattern gaseous detectors (MPGD), radially ranging from 3.3 cm to 77.5 cm. For $|\eta| > 1.1$, the tracking system consists of silicon disks followed by a large-area micromegas in the forward (proton/nucleus going) direction and all silicon disks in the backward (electron-going) direction. For the PID system, a time-of-flight detector and Cherenkov detector were used for particle identification at the middle and forward rapidity, respectively.

For the tracking system, a full GEANT4 simulation was performed with the latest design based on which the resolutions for the primary vertex position, distances from the tracks-to-tracks and from tracks-to-points, and track momentum, the tracking detector efficiencies are provided

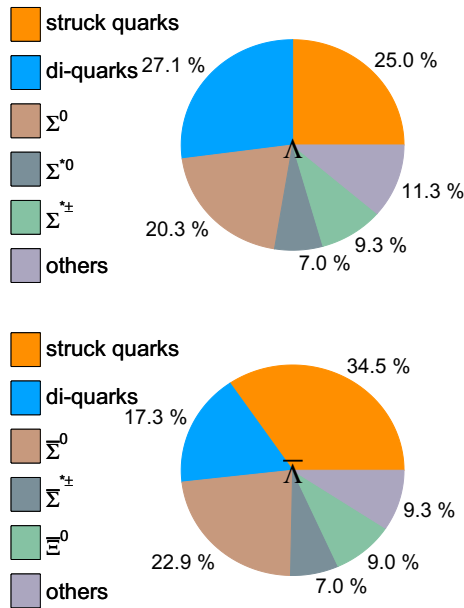


Fig. 4 (Color online) Origins of Λ and $\bar{\Lambda}$ with $x_F > 0$, $|\eta| < 3$ based on the PYTHIA event record

as a function of tracks p_T and η in Ref. [35] (Fig.4-9). In addition, a fast simulation framework was developed to simulate the detector responses learned from the GEANT4-base simulation. In this study, we followed the same fast simulation procedure described in Ref. [35]. A detailed GEANT4 simulation of the PID system was not available when this study was performed. To mimic the particle identification imperfection, a simplified ‘‘PID smearing’’ is included in the detector effect fast simulation. In principle, the PID efficiency correlates with the momentum of the particles. However, we employed a toy model to study the PID effect with a typical PID efficiency of 95% as follows. The identified π , K , or p have a 95% possibility of being correct and a 2.5% possibility of being one of the other two particles, respectively, as described by the following matrix:

$$\begin{bmatrix} \pi \\ K \\ p \end{bmatrix}_{\text{smearred}} = \begin{bmatrix} 0.95 & 0.025 & 0.025 \\ 0.025 & 0.95 & 0.025 \\ 0.025 & 0.025 & 0.95 \end{bmatrix} \begin{bmatrix} \pi \\ K \\ p \end{bmatrix}_{\text{truth}} \quad (2)$$

Here, 95% of the PID purity is specifically chosen, and a few other numbers are also checked for a complete study.

3 Lambda reconstruction

Similar to the method used in other experiments with a tracking detector, $\Lambda/\bar{\Lambda}$ reconstruction in this study was based on the topological structure of the decay channel with a large branching ratio, $\Lambda \rightarrow p\pi^-$ and $\bar{\Lambda} \rightarrow \bar{p}\pi^+$. Considering

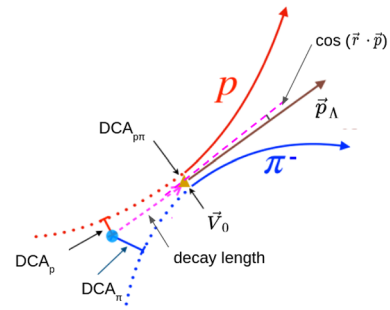


Fig. 5 Topology schematic diagram of the Λ production and its decay process through $\Lambda \rightarrow p\pi^-$

Λ as an example, Fig. 5 presents a schematic of the main topological features of its production and decay processes in a tracking detector. The blue dot at the bottom-left represents the ep scattering vertex, which is called the ‘‘primary vertex’’. $\Lambda/\bar{\Lambda}$ is emitted from the primary vertex, which then moves along the straight magenta dashed-line and decay at the ‘‘V0 vertex’’. The decay products $p\pi^-$ ($\bar{p}\pi^+$) travel along the helical lines with opposite bending directions in the magnetic field.

The reconstruction of $\Lambda/\bar{\Lambda}$ starts by pairing the proton and pion tracks with opposite charges. To select the $\Lambda/\bar{\Lambda}$ candidates and suppress random backgrounds, the following selection variables were considered:

- (1) The distance of closest approach (DCA) of the proton and pion tracks to the primary vertex. As indicated in Fig. 5, DCA_p and DCA_π from the signals should be significantly higher than those from the background because the parent $\Lambda/\bar{\Lambda}$ flies at certain distances from the primary vertex before its decay.
- (2) The DCA between paired proton and pion tracks. For the $\Lambda/\bar{\Lambda}$ signal, this variable should be consistent with zero within the track space resolution. The decay point (V0 vertex) is the midpoint of these two tracks in the closest approach, as indicated by the brown triangle in Fig. 5.
- (3) The decay length of $\Lambda/\bar{\Lambda}$ candidates, which is the distance between the primary vertex and the V0 vertex. The characteristic decay length of Λ hyperon $c\tau$ is 7.89 cm [2].
- (4) The angle between the $\Lambda/\bar{\Lambda}$ candidate momentum \vec{p} and its trajectory \vec{r} from the primary vertex. For the $\Lambda/\bar{\Lambda}$ directly produced from the primary vertex, the momentum direction is supposed to be along its trajectory from the primary vertex. Correspondingly, $\cos(\vec{r} \cdot \vec{p})$ should be significantly close to one.

Fig. 6 (Color online) Distributions of the topological variables for the $\Lambda/\bar{\Lambda}$ signal (red) and background (blue), respectively

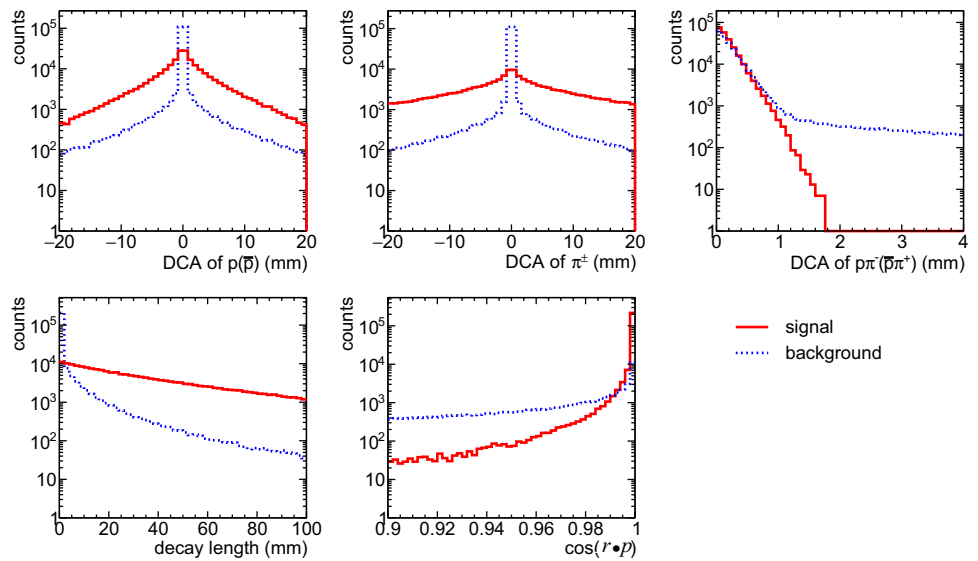


Table 1 Summary of the topological criteria for $\Lambda/\bar{\Lambda}$ reconstruction

Variables	Cut condition
DCA_p	> 0.1 mm
DCA_π	> 0.5 mm
DCA of $p\pi$ pair	< 0.8 mm
Decay length	> 1.5 mm
$\cos(\vec{r} \cdot \vec{p})$	> 0.95

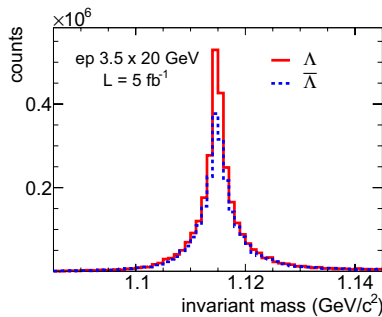


Fig. 7 (Color online) Invariant mass distributions of the Λ and $\bar{\Lambda}$ candidates passing all the selection criteria

To determine the selection criteria quantitatively, the distributions of the proton-pion pairs from pure $\Lambda/\bar{\Lambda}$ samples were compared with the proton-pion pairs from the background, which are shown in Fig. 6. Based on the comparisons, a set of selection criteria was optimized to balance the background fraction and the $\Lambda/\bar{\Lambda}$ reconstruction efficiency to retain as many signals as possible while maintaining the background fraction at a relatively low level. The numerical cutting conditions are presented in Table 1.

By implementing the aforementioned selection criteria, we successfully obtain a clean sample of $\Lambda/\bar{\Lambda}$ candidates.

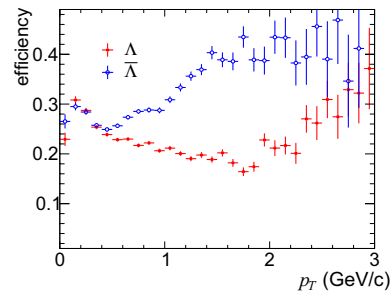


Fig. 8 (Color online) Reconstruction efficiency of Λ and $\bar{\Lambda}$ as a function of p_T after all the selection criteria were applied

The invariant mass spectrum of the $\Lambda/\bar{\Lambda}$ candidates with kinematics cuts of $x_F > 0$, $|\eta| < 3$, and $z_\Lambda > 0.1$ (fractional momentum of $\Lambda/\bar{\Lambda}$ is defined as $z_\Lambda \equiv \frac{P \cdot p_\Lambda}{P \cdot q}$), as shown in Fig. 7. Here, the histograms are scaled to an integral luminosity of 5 fb^{-1} , which corresponds to approximately one month of EicC data acquisition. With all the selection criteria applied, more Λ than $\bar{\Lambda}$ are reconstructed owing to the enhancement of the baryon number. There was a clean Gaussian signal peak with a very limited background. The residual background mainly originated from the random combinations of oppositely charged particles and particle mis-identification. The invariant mass distributions of these backgrounds were expected to be linear. Using the typical sideband method, the residual background fraction was estimated to be 2.6% for Λ and 3.0% for $\bar{\Lambda}$. The signal mass window was set to be within the 3σ -width of the Gaussian fit, which was (1.106, 1.124) GeV/c^2 . The sidebands are limited to the regions distant from the mass window to avoid signal fluctuations but are insufficiently distant to escape

from the signal peak. The left side-band was (1.083, 1.093) GeV/c² and the right side-band was (1.137, 1.147) GeV/c². The background under the signal peak was estimated as the sum of the two sidebands normalized to the signal window. As indicated in Sect. 2, the sensitivity of the $\Lambda/\bar{\Lambda}$ reconstruction to the PID performance is assessed by varying the PID “purity” number. For a 100% PID purity, the residual background fraction is 1.7%, whereas for a 90% purity, the residual background fraction increases to 3.4%, which is still under good control.

Figure 8 presents the Λ and $\bar{\Lambda}$ reconstruction efficiencies versus the transverse momentum. The reconstruction efficiency involves several effects, including the topological cuts, detector acceptance, and track efficiency, which depend on track p_T and track η . For $\Lambda/\bar{\Lambda}$ with a large decay length, the number of tracking detector layers through which the daughter tracks pass decreases, as does the tracking efficiency. The efficiency at a significantly low p_T is limited by the detector acceptance owing to the magnetic field. Owing to low transverse momentum in the forward region (large $|\eta|$), the efficiency decreases significantly. As already shown in Fig. 3, more Λ than $\bar{\Lambda}$ are produced at a large pseudorapidity where the reconstruction efficiency is low, which leads to a significantly higher efficiency of $\bar{\Lambda}$ compared Λ to $p_T > 0.5$ GeV/c. When p_T is larger than 2 GeV/c, the efficiency of Λ reconstruction increases and approaches $\bar{\Lambda}$ because Λ at the middle rapidity starts to dominate its production.

4 Spontaneous transverse polarization

In this section, we take the $\Lambda/\bar{\Lambda}$ spontaneous transverse polarization as an example to explore the physics potential of EicC. The theoretical calculations and statistical projections based on our simulation results are as follows.

The QCD formalism is used to describe Λ spontaneous transverse polarization P_Λ in the semi-inclusive DIS process, $e^-(l) + p(P) \rightarrow e^-(l') + \Lambda(p_\Lambda, \mathbf{S}_{\Lambda\perp}) + X$. The Trento convention [36] is followed in the calculation, where the virtual photon moves in the positive z direction and the proton moves in the negative z direction, and the differential cross-section can be expressed as follows [37, 38]:

$$\frac{d\sigma(\mathbf{S}_{\Lambda\perp})}{dx_B dy dz_\Lambda d^2\mathbf{p}_{\Lambda\perp}} = \frac{4\pi\alpha_{em}^2}{yQ^2} \frac{y^2}{2(1-\epsilon)} \left(1 + \frac{\gamma^2}{2x_B}\right) \left\{ F_{UU} + |\mathbf{S}_{\Lambda\perp}| \sin(\phi_{S_\Lambda} - \phi_\Lambda) F_{UT}^{\sin(\phi_{S_\Lambda} - \phi_\Lambda)} + \dots \right\}, \tag{3}$$

where $\gamma = 2x_B M/Q$ and $Q^2 = -q^2$, $x_B = \frac{Q^2}{2P \cdot q}$, $y = \frac{P \cdot q}{P \cdot l}$, $z_\Lambda = \frac{P \cdot p_\Lambda}{P \cdot q}$ are Lorentz invariant variables, and $\mathbf{S}_{\Lambda\perp}$, $\mathbf{p}_{\Lambda\perp}$ are the transverse spin vector and transverse momentum of the Λ hyperon, respectively. $F_{AB} = F_{AB}(x_B, z_\Lambda, \mathbf{p}_{\Lambda\perp}, Q)$, where the subscripts indicate the polarization of the proton and Λ ,

respectively. F_{UU} is the spin-averaged structure function and $F_{UT}^{\sin(\phi_{S_\Lambda} - \phi_\Lambda)}$ is the spin-dependent term that contributes to the spontaneous transverse polarization. The experimentally measured polarization P_Λ is related to the structure functions as follows:

$$P_\Lambda = \frac{F_{UT}^{\sin(\phi_{S_\Lambda} - \phi_\Lambda)}}{F_{UU}}. \tag{4}$$

Within the usual transverse momentum distribution (TMD) factorization at the leading twist, the structure functions can be expressed as follows:

$$\begin{aligned} F_{UU} &= \int d^2\mathbf{p}_\perp d^2\mathbf{k}_\perp \delta^2(z_\Lambda \mathbf{p}_\perp + \mathbf{k}_\perp - \mathbf{p}_{\Lambda\perp}) \\ &\quad \times \sum_q e_q^2 f_{1q}(x_B, \mathbf{p}_\perp^2; Q) D_{1q}^\Lambda(z_\Lambda, \mathbf{k}_\perp^2; Q), \\ F_{UT}^{\sin(\phi_{S_\Lambda} - \phi_\Lambda)} &= \int d^2\mathbf{p}_\perp d^2\mathbf{k}_\perp \delta^2(z_\Lambda \mathbf{p}_\perp + \mathbf{k}_\perp - \mathbf{p}_{\Lambda\perp}) \\ &\quad \times \sum_q e_q^2 \frac{\hat{\mathbf{p}}_{\Lambda\perp} \cdot \mathbf{k}_\perp}{z_\Lambda M_\Lambda} f_{1q}(x_B, \mathbf{p}_\perp^2; Q) D_{1Tq}^{\perp\Lambda}(z_\Lambda, \mathbf{k}_\perp^2; Q), \end{aligned} \tag{5}$$

where \mathbf{p}_\perp and \mathbf{k}_\perp denote the transverse momentum of the quark relative to the initial proton and the transverse momentum of Λ relative to its parent quark, respectively.

The TMDs were parameterized using the typical Gaussian form as the product of the collinear functions and Gaussian widths:

$$\begin{aligned} f_{1q}(x_B, \mathbf{p}_\perp^2; Q) &= f_{1q}(x_B, Q) \frac{e^{-\mathbf{p}_\perp^2 / \langle p_\perp^2 \rangle}}{\pi \langle p_\perp^2 \rangle}, \\ D_{1q}^\Lambda(z_\Lambda, \mathbf{k}_\perp^2; Q) &= D_{1q}^\Lambda(z_\Lambda, Q) \frac{e^{-\mathbf{k}_\perp^2 / \langle k_\perp^2 \rangle}}{\pi \langle k_\perp^2 \rangle}, \\ D_{1Tq}^{\perp\Lambda}(z_\Lambda, \mathbf{k}_\perp^2; Q) &= D_{1Tq}^{\perp\Lambda}(z_\Lambda, Q) \frac{e^{-\mathbf{k}_\perp^2 / \langle M_D^2 \rangle}}{\pi \langle M_D^2 \rangle}, \end{aligned} \tag{6}$$

where $\langle p_\perp^2 \rangle = 0.61$, $\langle k_\perp^2 \rangle = 0.19$ and $\langle M_D^2 \rangle = 0.118$ are the corresponding Gaussian widths obtained from Ref. [39, 40]. In this analysis, we used the CT18NLO [41] parameterization for the collinear PDF and the DSV [42] and AKK08 [43] parameterizations for the collinear unpolarized FF. Both parameterizations describe experimental data but significantly differ, with AKK08 including substantial isospin sym-

metry violations and DSV parameterization conserving it. In addition, the universality of the polarizing FF $D_{1Tq}^{\perp\Lambda}$ has been proven [44–46]. Similarly, $D_{1Tq}^{\perp\Lambda}$ as a modulation of D_{1q}^Λ by an additional collinear function, is described by two different parameterizations: CLPSW [47], which considers

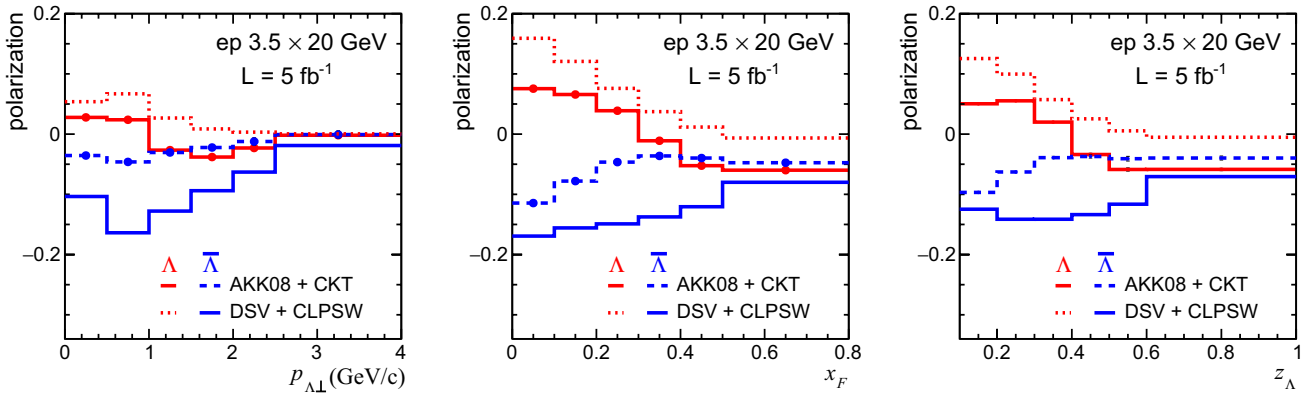


Fig. 9 Statistical projection with the theoretical predictions for the Λ and $\bar{\Lambda}$ polarization in the ep collisions at EicC. The projected statistical errors are smaller than those of the marker, and are thus invisible

isospin symmetry, and CKT, which allows isospin symmetry violations [40]. Future EicC will provide an ideal place to test the Λ isospin symmetry of FFs. In our study, we employed these different parameterizations to calculate and compare the polarization observables.

Using the parameterizations for the TMDs in Eq. (6), the spontaneous transverse polarization of Λ in Eq.(4) can be expressed in the following analytical form:

$$\begin{aligned}
 &P_\Lambda(x_B, z_\Lambda, \mathbf{p}_{\Lambda\perp}, Q) \\
 &= \frac{\sum_q e_q^2 f_{1q}(x_B, Q) D_{1Tq}^{\perp\Lambda}(z_\Lambda, Q) (\langle k_\perp^2 \rangle + z_\Lambda^2 \langle p_\perp^2 \rangle)}{\sum_q e_q^2 f_{1q}(x_B, Q) D_{1q}^\Lambda(z_\Lambda, Q) (\langle M_D^2 \rangle + z_\Lambda^2 \langle p_\perp^2 \rangle)^2} \quad (7) \\
 &\times \frac{\langle M_D^2 \rangle \mathbf{p}_{\Lambda\perp}}{z_\Lambda M_\Lambda} e^{\left\{ \frac{p_{\Lambda\perp}^2}{\langle k_\perp^2 \rangle + z_\Lambda^2 \langle p_\perp^2 \rangle} - \frac{p_{\Lambda\perp}^2}{\langle M_D^2 \rangle + z_\Lambda^2 \langle p_\perp^2 \rangle} \right\}}.
 \end{aligned}$$

Using this expression, we can estimate the magnitude of P_Λ in SIDIS. Considering $Q^2 = 5 \text{ GeV}^2$, P_Λ is plotted as a function of $\mathbf{p}_{\Lambda\perp}$ in Fig. 9. The results were obtained for different values covered by the kinematic range of the future EicC. To obtain the P_Λ dependence on the Feynman variable x_F , x_F was parameterized as a function of the Lorentz-invariant variables (x_B, z_Λ, Q) through a kinematic transformation as follows:

$$\begin{aligned}
 x_F = &\frac{-z_\Lambda Q^2}{M[x_B M^2 + (1 - x_B) Q^2]} \left[\sqrt{Q^2 + \frac{Q^4}{4x_B^2 M^2}} \right. \\
 &\left. + \left(M + \frac{Q^2}{2x_B M} \right) \sqrt{\frac{4x_B^2 M^2 (M_\Lambda^2 + \mathbf{p}_{\Lambda\perp}^2)}{z_\Lambda^2 Q^4} - 1} \right]. \quad (8)
 \end{aligned}$$

Using Eq.(7,8) and integrating over $\mathbf{p}_{\Lambda\perp}$, the results for the x_F - and z_Λ -dependent P_Λ were plotted in Fig. 9.

The statistical projection of $\Lambda/\bar{\Lambda}$ polarization is based on an integrated luminosity of 5 fb^{-1} , which is the same size as

the data sample, as shown in Fig. 7. The statistical uncertainties follow the equation format of $\delta P \approx \frac{1}{\alpha_\Lambda \sqrt{N}/3}$ based on the polarization extraction procedure. The Λ and $\bar{\Lambda}$ projected precision versus $p_{\Lambda\perp}$, x_F , and z_Λ are shown in Fig. 9 along with the theoretical predictions. The size of the error bars is smaller than the marker size and thus are invisible. Depending on the statistics in the different bins, the errors ranged from 0.002 to 0.007.

5 Summary and outlook

EicC is the proposed next-generation nuclear physics facility, which is expected to provide unique opportunities for precisely studying the 3-dimensional nucleon structure, nuclear partonic structures, and exotic hadron states, etc. The Lambda hyperon, which serves as a natural final state polarimeter, is a powerful tool for studying the nucleon spin structure and spin effect in the fragmentation process. The $\Lambda(\bar{\Lambda})$ measurements at EicC are of special importance and interest.

Based on the conceptual design of the EicC tracking system and GEANT4 simulation, we performed a detailed study of $\Lambda(\bar{\Lambda})$ production and reconstruction. In addition, taking spontaneous transverse polarization as an example, theoretical predictions were provided as functions of different kinematic variables, along with the statistical projections with one month of data obtained at EicC. We found that measurements using the EicC data obtained for only one month of operation based on the current accelerator design could provide distinguishable constraints for different parameterizations of the fragmentation functions.

EicC is designed to have both beams polarized, and the $\Lambda(\bar{\Lambda})$ polarization transferred either from the lepton or the proton beam can provide important constraints on the

spin-dependent PDFs and FFs in both co-linear and transverse momentum-dependent frameworks. More observables will be studied in the future, where decay contributions from heavier particles and a more realistic PID can be further investigated.

Acknowledgements We thank Tian-Bo Liu for the valuable discussions on the theoretical calculations. We thank the EicC tracking and heavy flavor working groups for their technical support with the detector simulation and useful suggestions on the analyses.

Author contributions All authors contributed to the study conception and design. Material preparation, data collection and analysis were performed by Zhaohuizi Ji, Xiao-Yan Zhao, Ai-Qiang Guo, Qing-Hua Xu, and Jin-Long Zhang. The first draft of the manuscript was written by Zhaohuizi Ji and Xiao-Yan Zhao and all authors commented on previous versions of the manuscript. All authors read and approved the final manuscript.

Data availability The data that support the findings of this study are openly available in Science Data Bank at <https://www.doi.org/10.57760/sciencedb.j00186.00271> and <https://cstr.cn/31253.11.sciencedb.j00186.00271>.

Declaration

Conflict of interest The authors declare that they have no competing interests.

References

1. T.D. Lee, C.N. Yang, General partial wave analysis of the decay of a hyperon of spin $1/2$. *Phys. Rev.* **108**, 1645–1647 (1957). <https://doi.org/10.1103/PhysRev.108.1645>
2. R.L. Workman, V.D. Burkert, V. Crede et al. (Particle Data Group), Review of particle physics. *PTEP* **2022**, 083C01 (2022). <https://doi.org/10.1093/ptep/ptac097>
3. G. Bunce, R. Handler, R. March et al., Λ^0 hyperon polarization in inclusive production by 300-GeV protons on beryllium. *Phys. Rev. Lett.* **36**, 1113–1116 (1976). <https://doi.org/10.1103/PhysRevLett.36.1113>
4. G.L. Kane, J. Pumplin, W. Repko, Transverse quark polarization in large- p_T reactions, e^+e^- jets, and lepton production: a test of quantum chromodynamics. *Phys. Rev. Lett.* **41**, 1689–1692 (1978). <https://doi.org/10.1103/PhysRevLett.41.1689>
5. D. Buskulic, I. De Bonis, D. Decamp et al., (ALEPH Collaboration), measurement of Λ polarization from Z decays. *Phys. Lett.* **374**, 319–330 (1996). [https://doi.org/10.1016/0370-2693\(96\)00300-0](https://doi.org/10.1016/0370-2693(96)00300-0)
6. K. Ackerstaff, G. Alexander, J. Allison et al., (OPAL Collaboration), Polarization and forward-backward asymmetry of Λ baryons in hadronic Z^0 decays. *Eur. Phys. J. C* **2**, 49–59 (1998). <https://doi.org/10.1007/s100520050123>
7. Y. Guan, A. Vossen, I. Adachi et al., (Belle Collaboration), Observation of transverse $\Lambda/\bar{\Lambda}$ hyperon polarization in e^+e^- annihilation at Belle. *Phys. Rev. Lett.* **122**, 042001 (2019). <https://doi.org/10.1103/PhysRevLett.122.042001>
8. M.R. Adams, M. Aderholz, S. Aid et al., (E665 Collaboration), Λ and $\bar{\Lambda}$ polarization from deep inelastic muon scattering. *Eur. Phys. J. C* **17**, 263–267 (2000). <https://doi.org/10.1007/s100520000493>
9. P. Astier, D. Autiero, A. Baldisseri et al., (NOMAD Collaboration), Measurement of the Λ polarization in ν_μ charged current interactions in the NOMAD experiment. *Nucl. Phys. B* **588**, 3–36 (2000). [https://doi.org/10.1016/S0550-3213\(00\)00503-4](https://doi.org/10.1016/S0550-3213(00)00503-4)
10. A. Airapetian, N. Akopov, M. Amarian et al., (HERMES Collaboration), Measurement of longitudinal spin transfer to Λ hyperons in deep-inelastic lepton scattering. *Phys. Rev. D* **64**, 112005 (2001). <https://doi.org/10.1103/PhysRevD.64.112005>
11. B.I. Abelev, M.M. Aggarwal, Z. Ahammed et al., (STAR Collaboration), Longitudinal spin transfer to Λ and $\bar{\Lambda}$ hyperons in polarized proton-proton collisions at $\sqrt{s} = 200$ GeV. *Phys. Rev. D* **80**, 111102 (2009). <https://doi.org/10.1103/PhysRevD.80.111102>
12. J. Adam, L. Adamczyk, J.R. Adams et al., (STAR Collaboration), Improved measurement of the longitudinal spin transfer to Λ and $\bar{\Lambda}$ hyperons in polarized proton-proton collisions at $\sqrt{s} = 200$ GeV. *Phys. Rev. D* **98**, 112009 (2018). <https://doi.org/10.1103/PhysRevD.98.112009>
13. J. Adam, L. Adamczyk, J.R. Adams et al., (STAR Collaboration), Transverse spin transfer to Λ and $\bar{\Lambda}$ hyperons in polarized proton-proton collisions at $\sqrt{s} = 200$ GeV. *Phys. Rev. D* **98**, 091103 (2018). <https://doi.org/10.1103/PhysRevD.98.091103>
14. L. Adamczyk, J.K. Adkins, G. Agakishiev et al., (STAR Collaboration), Global Λ hyperon polarization in nuclear collisions. *Nature* **548**, 62–65 (2017). <https://doi.org/10.1038/nature23004>
15. M.S. Abdallah, B.E. Aboona, J. Adam et al., (STAR Collaboration), Pattern of global spin alignment of ϕ and K^{*0} mesons in heavy-ion collisions. *Nature* **614**, 244–248 (2023). <https://doi.org/10.1038/s41586-022-05557-5>
16. X.N. Wang, Vector meson spin alignment by the strong force field. *Nucl. Sci. Tech.* **34**, 15 (2023). <https://doi.org/10.1007/s41365-023-01166-7>
17. J. Chen, Z.-T. Liang, Y.-G. Ma et al., Global spin alignment of vector mesons and strong force fields in heavy-ion collisions. *Sci. Bull.* **68**, 874 (2023). <https://doi.org/10.1016/j.scib.2023.04.001>
18. X. Sun, C.S. Zhou, J.H. Chen et al., Measurements of global polarization of QCD matter in heavy-ion collisions. *Acta Phys. Sin.* **72**(7), 072401 (2023). <https://doi.org/10.7498/aps.72.2022452> (in Chinese)
19. W. Lu, B.Q. Ma, The strange quark spin of the proton in semi-inclusive Λ lepton production. *Phys. Lett. B* **357**, 419–422 (1995). [https://doi.org/10.1016/0370-2693\(95\)00927-D](https://doi.org/10.1016/0370-2693(95)00927-D)
20. J. Ellis, D. Kharzeev, A. Kotzinian, The proton spin puzzle and Λ polarization in deep-inelastic scattering. *Z. Phys. C Part. Fields* **69**, 467–474 (1996). <https://doi.org/10.1007/BF02907428>
21. R.L. Jaffe, Polarized Λ in the current fragmentation region. *Phys. Rev. D* **54**, R6581–R6585 (1996). <https://doi.org/10.1103/PhysRevD.54.R6581>
22. B.Q. Ma, I. Schmidt, J. Soffer et al., Λ , $\bar{\Lambda}$ polarization and spin transfer in lepton deep inelastic scattering. *Eur. Phys. J. C* **16**, 657–664 (2000). <https://doi.org/10.1007/s100520000447>
23. J. Ellis, A. Kotzinian, D.V. Naumov, Intrinsic polarized strangeness and Λ^0 polarization in deep inelastic production. *Eur. Phys. J. C* **25**, 603–613 (2002). <https://doi.org/10.1140/epjc/s2002-01025-2>
24. S.S. Zhou, Y. Chen, Z.T. Liang et al., Longitudinal polarization of hyperon and anti-hyperon in semi-inclusive deep-inelastic scattering. *Phys. Rev. D* **79**, 094018 (2009). <https://doi.org/10.1103/PhysRevD.79.094018>
25. K.-B. Chen, Z.-T. Liang, Y.-K. Song et al., Longitudinal and transverse polarizations of Λ hyperon in unpolarized SIDIS and e^+e^- annihilation. *Phys. Rev. D* **105**, 034027 (2022). <https://doi.org/10.1103/PhysRevD.105.034027>
26. Z.B. Kang, J. Terry, A. Vossen et al., Transverse Λ production at the future Electron-Ion Collider. *Phys. Rev. D* **105**, 094033 (2022). <https://doi.org/10.1103/PhysRevD.105.094033>

27. X. Cao, L. Chang, N.B. Chang et al., Electron ion collider in China. *Nuclear Techniques* **43**(2), 020001 (2020) <https://doi.org/10.11889/j.0253-3219.2020.hjs.43.020001> (in Chinese)
28. D.P. Anderle, V. Bertone, X. Cao et al., Electron-ion collider in China. *Front. Phys.* **16**, 64701 (2021). <https://doi.org/10.1007/s11467-021-1062-0>
29. A. Lehrach, K. Aulenbacher, O. Boldt et al., The polarized electron-nucleon collider project ENC at GSI/FAIR. *J. Phys. Conf. Ser.* **295**, 012156 (2011). <https://doi.org/10.1088/1742-6596/295/1/012156>
30. J.L. Abelleira Fernandez, C. Adolphsen, A.N. Akay et al., A large hadron electron collider at CERN report on the physics and design concepts for machine and detector. *J. Phys. G Nucl. Part. Phys.* **39**, 075001 (2012). <https://doi.org/10.1088/0954-3899/39/7/075001>
31. R. Abdul Khalek, A. Accardi, J. Adam et al., Science requirements and detector concepts for the Electron-Ion Collider: EIC yellow report. *Nucl. Phys. A* **1026**, 122447 (2022). <https://doi.org/10.1016/j.nuclphysa.2022.122447>
32. PYTHIAeRHIC. <https://eic.github.io/software/pythia6.html>
33. T. Sjostrand, S. Mrenna, P. Skands, PYTHIA 6.4 physics and manual. *JHEP* **05**, 026 (2006). <https://doi.org/10.1088/1126-6708/2006/05/026>
34. M.R. Whalley, D. Bourilkov, R. C. Group, The les houches accord PDFs (LHAPDF) and LHAGLUE, [arXiv:hep-ph/0508110](https://arxiv.org/abs/hep-ph/0508110)
35. D.P. Anderle, A.Q. Guo, F. Hekhorn et al., Probing gluon distributions with D^0 production at the EicC. [arXiv: 2307.16135](https://arxiv.org/abs/2307.16135)
36. A. Bacchetta, U. D'Alesio, M. Diehl, C. Miller, Single-spin asymmetries: the trento conventions. *Phys. Rev. D* **70**, 117504 (2004). <https://doi.org/10.1103/PhysRevD.70.117504>
37. D. Boer, P.J. Mulders, Time-reversal odd distribution functions in lepton production. *Phys. Rev. D* **57**, 5780–5786 (1997). <https://doi.org/10.1103/PhysRevD.57.5780>
38. A. Bacchetta, M. Diehl, K. Goeke et al., Semi-inclusive deep inelastic scattering at small transverse momentum. *JHEP* **2007**, 093 (2007). <https://doi.org/10.1088/1126-6708/2007/02/093>
39. M. Anselmino, M. Boglione, J.O. Gonzalez H. et al., Unpolarised transverse momentum dependent distribution and fragmentation functions from SIDIS multiplicities. *J. High Energy. Phys* **2014**, 5 (2014). [https://doi.org/10.1007/JHEP04\(2014\)005](https://doi.org/10.1007/JHEP04(2014)005)
40. D. Callos, Z.-B. Kang, J. Terry, Extracting the transverse momentum dependent polarizing fragmentation functions. *Phys. Rev. D* **102**, 096007 (2020). <https://doi.org/10.1103/PhysRevD.102.096007>
41. T.-J. Hou, K.P. Xie, J. Gao et al., Progress in the CTEQ-TEA NNLO global QCD analysis. [arXiv:1908.11394](https://arxiv.org/abs/1908.11394)
42. D. de Florian, M. Stratmann, W. Vogelsang, QCD analysis of unpolarized and polarized Λ -baryon production in leading and next-to-leading order. *Phys. Rev. D* **57**, 5811–5824 (1998). <https://doi.org/10.1103/PhysRevD.57.5811>
43. S. Albino, B.A. Kniehl, G. Kramer, AKK update: improvements from new theoretical input and experimental data. *Nucl. Phys. B* **803**, 42–104 (2008). <https://doi.org/10.1016/j.nuclphysb.2008.05.017>
44. A. Metz, Gluon-exchange in spin-dependent fragmentation. *Phys. Lett. B* **549**, 139–145 (2002). [https://doi.org/10.1016/S0370-2693\(02\)02899-X](https://doi.org/10.1016/S0370-2693(02)02899-X)
45. S. Meißner, A. Metz, Partonic pole matrix elements for fragmentation. *Phys. Rev. Lett.* **102**, 172003 (2009). <https://doi.org/10.1103/PhysRevLett.102.172003>
46. D. Boer, Z.-B. Kang, W. Vogelsang et al., Test of the universality of Naive-time-reversal-odd fragmentation functions. *Phys. Rev. Lett.* **105**, 202001 (2010). <https://doi.org/10.1103/PhysRevLett.105.202001>
47. K.-B. Chen, Z.-T. Liang, Y.-L. Pan et al., Isospin symmetry of fragmentation functions. *Phys. Lett. B* **816**, 136217 (2021). <https://doi.org/10.1016/j.physletb.2021.136217>

Springer Nature or its licensor (e.g. a society or other partner) holds exclusive rights to this article under a publishing agreement with the author(s) or other rightsholder(s); author self-archiving of the accepted manuscript version of this article is solely governed by the terms of such publishing agreement and applicable law.